Dilepton as a possible signature for the baryon-rich quark-gluon plasma

L. H. Xia,* C. M. Ko, and C. T. Li
Cyclotron Institute and Center for Theoretical Physics, Texas A&M University, College Station, Texas 77843
(Received 31 July 1989)

In an expanding fireball model, we study dilepton production from high-energy heavy-ion collisions at the stopping regime. We find that the pion-pion annihilation gives the dominant contribution to the dilepton yield at invariant masses between $2m_\pi$ and 1 GeV. The total dilepton yield in this invariant mass region increases with the incident energy of the collision, but a saturation is seen once a baryon-rich quark-gluon plasma is formed in the initial stage.

I. INTRODUCTION

The ultimate goal of heavy-ion collisions at ultrarelativistic energies is to create a deconfined quark-gluon plasma.[1] It is hoped that during the initial stage of the collision, a region of high-energy density will be produced so that a transition from the hadronic matter to the quark-gluon plasma will take place. For future experiments at the proposed relativistic heavy-ion collider (RHIC) a baryon free quark-gluon plasma is expected to be created because of the increasing transparency of the nuclear matter with increasing collision energies.[2] At present, the CERN experiments at both 60 GeV/nucleon and 200 GeV/nucleon indicate that the incident projectile is not completely stopped by the target and a high-energy density of many GeV/fm^3 has been reached.[1] The observation of the suppressed production of the J/Ψ particle has already stimulated great excitements as it might be a possible evidence for the formation of a quark-gluon plasma.[3] However, it will not be considered as a definitive signature until a better understanding of the dissociation of J/Ψ by the hadronic particles is achieved.[4-6] For experiments carried out at the Brookhaven National Laboratory Alternating Gradient Synchrotron (AGS) at 14.5 GeV/nucleon,[7] the analysis of the final transverse energy distribution indicates that the projectile is indeed completely stopped by the target and that a hadronic matter of density about five times the normal nuclear matter density has been reached in the initial stage. Whether a baryon-rich quark-gluon plasma has been formed in such a collision is still uncertain. It has been argued in the past that the formation of a quark-gluon plasma may be signaled by an enhanced production of kaons relative to that of pions.[8] Data obtained at the AGS indeed show an enhancement of a factor of 4 for K^+/π^+ ratio compared with that from the proton-proton and the proton-nucleus collisions.[9] However, theoretical studies show that a substantial enhancement can be obtained by assuming either the formation of a quark-gluon plasma or a dense hadronic matter in the initial stage of the collision.[10,11] In view of the ambiguity associated with these observables as signatures for the quark-gluon plasma, the consideration of other observables will be very useful.

A very interesting suggestion in the past has been the dilepton. It was suggested that the disappearance of the rho peak in the dilepton invariance mass spectrum might signal the formation of a quark-gluon plasma.[12,13] Detailed studies including the proper treatment of the expansion dynamics, however, do not support such a possibility.[14] These studies are all concerned with the baryon free quark-gluon plasma that might be produced in future RHIC energies. At the AGS, energies in the range of about 15 GeV/nucleon, a dense hadronic matter will be formed if no quark-gluon plasma is created in the initial stage. In the hadronic matter, dileptons can be produced from both pn bremsstrahlung and the $\pi\pi$ annihilation. For dense hadronic matter at high temperatures, it has been shown in Refs. 15 and 16 that the contribution from the $\pi\pi$ annihilation is more significant than that from the pn bremsstrahlung for dileptons of invariant masses in the region of $2m_\pi$ to about 1 GeV, where m_π is the mass of pion. It is also found in Refs. 15–17 that the modification of the pion dispersion relation by the dense nuclear matter because of the strong p-wave πN interaction can lead to an enhanced production of dileptons at small invariant masses. This effect becomes more pronounced as the density of the hadronic matter increases. On the other hand, if a baryon-rich quark-gluon plasma is initially formed, then dileptons will be produced from the $q\bar{q}$ annihilation. After the hadronization of the quark-gluon plasma, dileptons can also be produced from the hadronic matter via the pn bremsstrahlung and the $\pi\pi$ annihilation. Since the total entropy cannot decrease during the transition, the final hadronic matter will be at a higher temperature and lower density than the initial quark-gluon matter.[18] If the quark-gluon plasma contributes mainly to dileptons with larger invariant masses, then we expect a reduced production of dileptons with low invariant masses, compared with the case without the formation of a quark-gluon plasma because of the low hadronic matter density after its hadronization. In this case, it is of interest to measure the total yield of dilepton with the invariant mass in the region of $2m_\pi$ to about 1 GeV as a function of the incident energy. The onset of a baryon-rich quark-gluon plasma is thus signaled by the appearance of a plateau in this excitation function.

To substantiate this conjecture, we have carried out calculations for dilepton production based on the hydrodynamical description of heavy-ion collisions. In Sec. II,

the nuclear phase diagram is introduced. The initial condition of the fireball and its hydrodynamical expansion are described in Sec. III. The kinetic processes and the hadronization model are discussed in Sec. IV. In Sec. V, the elementary dilepton production processes are discussed. The results for dilepton production from high-energy heavy-ion collisions are presented in Sec. VI. Conclusions are given in Sec. VII. A brief report of this work has already been published in Ref. 19.

II. NUCLEAR PHASE DIAGRAM

Based on the quantum chromodynamics, it is generally believed that the nuclear matter exists in a deconfined phase of quarks and gluons when its density and temperature are high. The determination of the nuclear phase diagram from the quantum chromodynamics is, however, a difficult task. Instead, we shall use a simplified model to construct the nuclear phase diagram. It is determined by considering both the hadronic and the quark-gluon matter as composed of noninteracting nonstrange particles with the latter supplemented by a bag constant. This model of the nuclear phase diagram has been used previously in Refs. 20 and 21. As pointed out in these references, the inclusion of strange particles affects the phase diagram only slightly. Since we shall look for qualitative signatures for the formation of a quark-gluon plasma, we believe that such a model will be sufficient in the present work. For completeness, we describe briefly in the following the construction of the nuclear phase diagram in this simple model.

A. Equation of state for quark-gluon phase

For the noninteracting quark-gluon matter consisting of the up and down quarks and the gluons, the quark density n_Q, the antiquark density $n_{\bar{Q}}$, and the gluon density n_G can be written as[22]

$$n_Q=\frac{d_Q}{2\pi^2}\int_0^\infty \frac{k^2dk}{e^{(k-\mu_q)/T}+1} , \tag{1a}$$

$$n_{\bar{Q}}=\frac{d_Q}{2\pi^2}\int_0^\infty \frac{k^2dk}{e^{(k+\mu_q)/T}+1} , \tag{1b}$$

$$n_G=\frac{d_G}{2\pi^2}\int_0^\infty \frac{k^2dk}{e^{k/T}-1}=16\zeta(3)T^3/\pi^2 , \tag{1c}$$

respectively. In the above, we have $\zeta(3)=1.202\,06$, the quark degeneracy $d_Q=12$, the gluon degeneracy $d_G=16$, the chemical potential μ_q for the quark, and the temperature T. The baryon number density is then given by

$$n_{b,q}=\tfrac{1}{3}(n_Q-n_{\bar{Q}})=\frac{2}{3}\left[\mu_q T^2+\frac{\mu_q^3}{\pi^2}\right] . \tag{2}$$

Also, the quark energy density e_Q, the antiquark energy density $e_{\bar{Q}}$, and the gluon energy density e_G are written as

$$e_Q=\frac{d_Q}{2\pi^2}\int_0^\infty \frac{k^3dk}{e^{(k-\mu_q)/T}+1} , \tag{3a}$$

$$e_{\bar{Q}}=\frac{d_Q}{2\pi^2}\int_0^\infty \frac{k^3dk}{e^{(k+\mu_q)/T}+1} , \tag{3b}$$

$$e_G=\frac{d_G}{2\pi^2}\int_0^\infty \frac{k^3dk}{e^{k/T}-1} , \tag{3c}$$

which lead to the total energy density in the quark-gluon plasma

$$\begin{aligned} e_q&=e_Q+e_{\bar{Q}}+e_G+B \\ &=\tfrac{37}{30}\pi^2T^4+3\mu_q^2T^2+\frac{3\mu_q^4}{2\pi^2}+B , \end{aligned} \tag{4}$$

where B is the bag constant. From the number and energy densities, the pressure and entropy densities of the quark-gluon plasma are given by

$$p_q=\tfrac{1}{3}(e_q-B)-B , \tag{5}$$

$$s_q=\frac{1}{T}(e_q+p_q-3\mu_q n_{b,q}) . \tag{6}$$

B. Equation of state for the hadronic phase

For the hadronic matter, we include only nonstrange stable hadrons (nucleon, pion, and eta) and their resonances (Δ's, N^*'s, ρ, and ω) as in Refs. 20 and 21. In the case that their interactions can be neglected, the number density n_i, the energy density e_i, and the pressure p_i of the ith particle are given by

$$n_i=\frac{d_i}{2\pi^2}\int_0^\infty \frac{k^2dk}{e^{(\epsilon_i-\mu_i)/T}\pm 1} , \tag{7}$$

$$e_i=\frac{d_i}{2\pi^2}\int_0^\infty \frac{\epsilon_i k^2dk}{e^{(\epsilon_i-\mu_i)/T}\pm 1} , \tag{8}$$

$$p_i=\frac{d_i}{6\pi^2}\int_0^\infty \frac{\epsilon_i^{-1}k^4dk}{e^{(\epsilon_i-\mu_i)/T}\pm 1} , \tag{9}$$

where $\epsilon_i=(k^2+m_i^2)^{1/2}$. In the above, $+$ is for fermions and $-$ for bosons. The d_i indicates the degeneracy, while the chemical potential is denoted by μ_i. For baryons, we have $\mu_i=b_i\mu_b$, where b_i is the baryon number and μ_b is the baryon chemical potential. The total baryon number and energy density, as well as the pressure of the hadronic matter are then given by $n_{b,h}=\sum_i b_i n_i$, $e_h=\sum_i e_i$, and $p_h=\sum_i p_i$, respectively. From these thermodynamical quantities, the entropy density is

$$s_h=\frac{1}{T}(e_h+p_h-\mu_b n_{b,h}) .$$

C. Nuclear phase diagram

The critical temperature and density at which the transition between the quark-gluon and hadronic phases occurs is determined by the Gibb's condition that the two phases are in the thermal, chemical, and mechanical equilibrium, i.e., $T_h=T_q$, $\mu_b=3\mu_q$, and $p_h=p_q$. As shown by Heinz *et al.*,[23] there exists however a range of values of

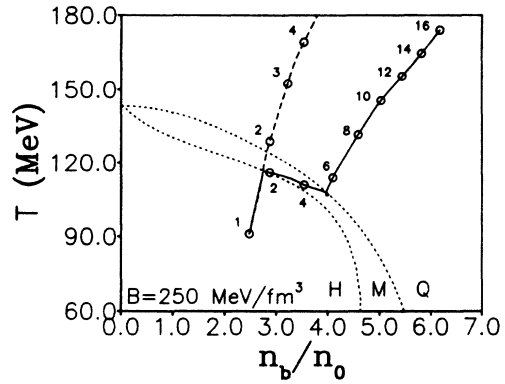

FIG. 1. Nuclear phase diagram in the space of temperature T and the baryon density n_b for a bag constant of 250 MeV/fm^3. The entry points from heavy-ion collisions between identical nuclei are shown by the solid curve. The numbers near the circles denote the incident energies in GeV per nucleon. The dashed curve corresponds to the entry points in a purely hadronic scenario.

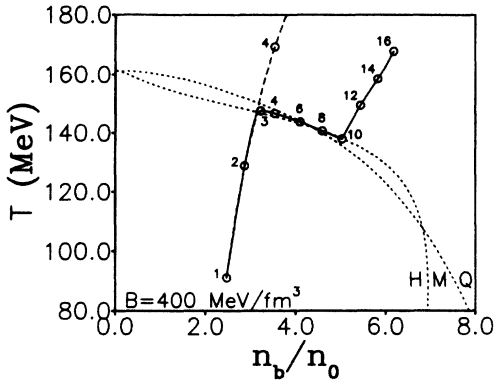

FIG. 3. Same as Fig. 1 for a bag constant of 400 MeV/fm^3.

B and μ_q for which the mechanical equilibrium condition cannot be satisfied, and the hadronic phase never decays into the quark-gluon phase. The origin for this pathological behavior is the assumption of noninteracting pointlike hadrons. To overcome this difficulty, they have included a finite proper volume for hadrons so that the quantities $n_{b,h}$, e_h, p_h, and s_h are all multiplied by the correction factor $C=1/(1+e_h/4B)$, where B is the bag constant. This limits the energy density in the hadronic phase to $4B$. However, there is a concern about the consistency of adding this finite volume in the calculation of the thermodynamical quantities. This will not be a serious problem for us as this phase diagram is meant to illustrate the possible scenarios that might happen in high-energy heavy-ion reactions and probably differs in details when more sophisticated models such as those of Refs. 18 and 24 are used.

Once the critical temperature T^c, the critical chemical potential μ_b^c, and the critical pressure p^c are determined, other critical values such as $n_{b,h}^c$, $n_{b,q}^c$, e_h^c, s_h^c, and s_q^c, can be evaluated. In Fig. 1, we show the phase diagram in the space of the temperature and baryon density for a bag constant $B=250$ MeV/fm^3, while in Fig. 2 the phase diagram in the space of the energy and baryon densities is shown for the same value of bag constant. The critical energy density for the formation of the quark-gluon plasma is only slightly above 1 GeV/fm^3. The formation of a mixed phase of the quark-gluon and hadronic matter occurs at even lower energy densities. Similar phase diagrams for a bag constant of $B=400$ MeV/fm^3 are shown in Figs. 3 and 4. The critical energy density in this case is close to 2 GeV/fm^3.

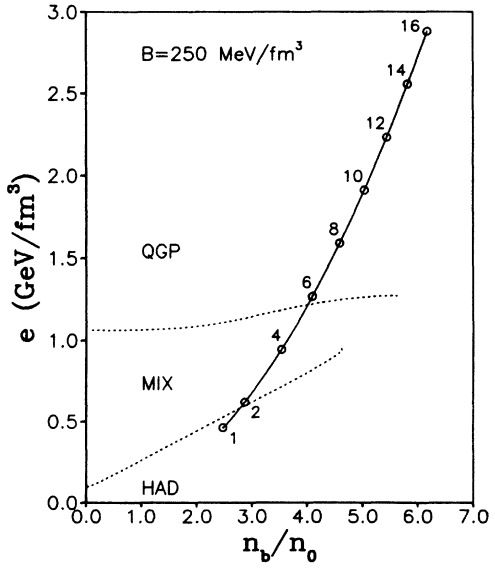

FIG. 2. Same as Fig. 1 for nuclear phase diagram in the space of the energy density e and the baryon density n_b.

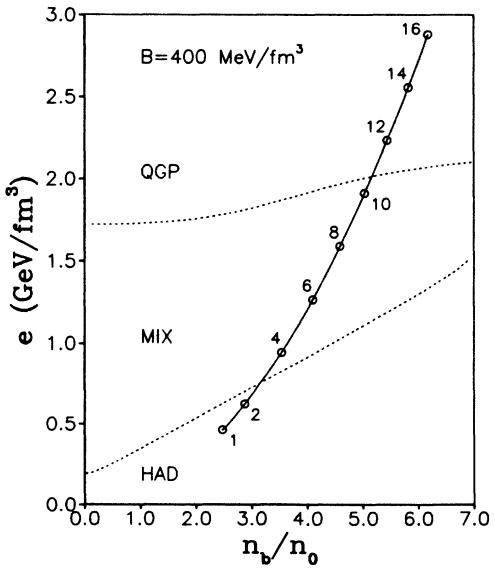

FIG. 4. Same as Fig. 2 for a bag constant of 400 MeV/fm^3.

III. INITIAL CONDITIONS AND THE EXPANSION DYNAMICS

A. Determination of the initial phase

We assume that a baryon-rich fireball is formed in the collision of two heavy ions. To estimate the size of the fireball, it is reasonable to assume for collisions at high energies that the projectile sweeps through the target on a straight trajectory and moves forward together with the target nucleons that are in the volume traversed by the projectile. Using a uniform density for both the projectile and the target, we obtain that at zero impact parameter the number of participants for two ions with mass numbers A_1, A_2 ($A_1 \leq A_2$) are given by

$$N_1 = A_1 , \tag{10a}$$

$$N_2 = A_2\{1-[1-(A_1/A_2)^{2/3}]^{3/2}\} . \tag{10b}$$

The initial density of the fireball is estimated by taking its volume to be the arithmetic mean of the two Lorentz contracted volumes, i.e.,

$$n_b^0 = \frac{2(N_1+N_2)}{\frac{N_1}{\gamma_1}+\frac{N_2}{\gamma_2}} n_0 , \tag{11}$$

where n_0 is normal nuclear density; γ_1 and γ_2 are the Lorentz factors associated with the projectile and the target, respectively. For the collision between two identical nuclei, we have $N_1=N_2$ and $\gamma_1=\gamma_2=\gamma$ and obtain $n_b^0=2\gamma n_0$. The inclusion of compressions via the shock model as in Ref. 25 will lead to an even larger initial density. If the incident energy per particle is E, then the center-of-mass energy per baryon in the fireball is

$$w = m_N[N_1^2+N_2^2+2N_1N_2(1+E/m_N)]^{1/2} ,$$

with m_N the nucleon mass. The initial energy density of the fireball is thus $e^0=wn_b^0$.

If the fireball is initially in either the hadronic or the quark-gluon phase, its thermodynamical property, such as temperature, pressure, and chemical potential, can be easily determined from the initial baryon and energy densities. If the initial state is in the mixed phase, we need to know the fraction f_q^0 of quark-gluon plasma in the fireball. With the initial temperature of the mixed state denoted by T^0, the baryon densities $n_{b,q}(T^0)$ of the quark-gluon plasma and $n_{b,h}(T^0)$ of the hadronic matter in the mixed phase can be determined from the critical lines in the phase diagram of Fig. 1. From these baryon densities, the energy densities $e_q(T^0)$ of the quark-gluon plasma and $e_h(T^0)$ of the hadronic matter in the mixed phase can also be determined. The unknown initial temperature T^0 and the volume fraction f_q^0 of the mixed phase can thus be extracted from the following equations:

$$n_b^0 = f_q^0 n_{b,q}(T^0)+(1-f_q^0)n_{b,h}(T^0) , \tag{12a}$$

$$e^0 = f_q^0 e_q(T^0)+(1-f_q^0)e_h(T^0) . \tag{12b}$$

These entry points are shown in Figs. 1 and 2 by the open circles for the case of $B=250$ MeV/fm^3. The numbers near the circles stand for values of the energy per nucleon in units of GeV/nucleon. We see from the figures that the initial stage is in the hadronic phase for $E/A<2$ GeV, in the mixed phase for 2 GeV $\leq E/A<6$ GeV, and in the quark-gluon phase for $E/A \geq 6$ GeV. In Fig. 1, we also show by the dashed curve the entry points in a purely hadronic scenario. Similarly, they are shown in Figs. 3 and 4 for a bag constant of $B=400$ MeV/fm^3. In this case, the initial stage is in hadronic phase for $E/A<3$ GeV, in the mixed phase for 3 GeV $\leq E/A<11$ GeV, and in the quark-gluon phase for $E/A \geq 11$ GeV. Although there are differences between the two cases, the same results for the signature for quark-gluon plasma to be discussed later will be obtained.

B. Hydrodynamical expansion and kinetic equations

To model the fireball expansion we use the hydrochemical model of Biro *et al.*,[26] in which the fireball is assumed to be in thermal equilibrium and the thermal energy in the fireball is converted to the collective flow energy via the relativistic hydrodynamical equations that are further coupled to the rate equations

$$\partial_\mu T^{\mu 0}=0 , \tag{13a}$$

$$u_\nu \partial_\mu T^{\mu\nu}=0 , \tag{13b}$$

$$\partial_\mu(n_i u^\mu)=\psi_i , \tag{13c}$$

where $T^{\mu\nu}$ is the energy-momentum tensor and is given by

$$T^{\mu\nu}=(e+p)u^\mu u^\nu - p g^{\mu\nu} . \tag{14}$$

In the above, e and p are, respectively, the energy density and pressure, $g^{\mu\nu}$ is the standard metric tensor, and u^μ is the four velocity defined by $u^\mu=\gamma(1,\mathbf{u})$ with $\mathbf{u}$ the local velocity and $\gamma=1/(1-u^2)^{1/2}$ the associated Lorentz factor; ψ_i is the source term in the rate equations. Taking the spatial average of these equations for a uniform density distribution, we obtain

$$\frac{1}{V}\frac{d}{dt}[V(e\langle\gamma^2\rangle+p\langle\gamma^2u^2\rangle)]=0 , \tag{15a}$$

$$\frac{1}{V}\frac{d}{dt}[Vs\langle\gamma\rangle]=-\frac{1}{T}\sum_i \mu_i\psi_i , \tag{15b}$$

$$\frac{1}{V}\frac{d}{dt}[Vn_i\langle\gamma\rangle]=\psi_i , \tag{15c}$$

where s denotes the entropy density in the fireball. As in Ref. 26, we assume that the fireball expansion is isotropic and use the scaling *Ansätze* for the local radial velocity

$$\gamma u = \left[\frac{r}{R}\right]^n \dot{\tilde{R}} , \tag{16}$$

where r is the radial distance, R is the radius of the fireball, and $\dot{\tilde{R}}=\dot{R}/(1-\dot{R}^2)^{1/2}$ The exponent n is taken as a parameter. This leads to

$$\langle\gamma^2u^2\rangle=\langle\gamma^2\rangle-1=\frac{3}{2n+3}\dot{\tilde{R}}^2 , \tag{17a}$$

$$\langle\gamma\rangle=1+3\sum_{j=1}^{\infty}\frac{(-1)^{j+1}(2j-1)!!}{(2j-1)(2nj+3)(2j)!!}\dot{R}^{2j}\ . \quad (17b)$$

Using Eq. (16), we can rewrite Eq. (15a) as

$$V\left[e+(e+p)\frac{3}{2n+3}\dot{\hat{R}}^{2}\right]=E_0\ , \quad (18)$$

where E_0 is the total energy of the initial fireball and is a conserved quantity.

C. Phase transition from the quark-gluon plasma to the hadronic matter

If the fireball is initially in the hadronic phase, the system will simply expand until it reaches the freezeout density at which the mean free path of the particles is comparable to the size of the fireball. On the other hand, if the fireball is initially in the quark-gluon phase, its temperature and pressure decrease during the expansion and eventually it reaches the boundary of the phase diagram and makes a transition to the hadronic matter. In Fig. 5, the solid curve shows the trajectory in the phase diagram of Fig. 1 along which the system evolves during the expansion for the collision of symmetric systems at an incident energy of 14 GeV/nucleon. From Fig. 1, we see that the initial density is about $6n_0$ and the fireball is thus initially in the quark-gluon phase. The system reaches the boundary of the quark-gluon plasma at point 1 in the figure. From the conservation of baryon number and entropy,[20,21] we can determine the trajectory of the system in the mixed phase. It ends at point 2 on the critical line that separates the mixed phase from the hadronic phase. The rate for hadronization is not known and will be taken as a parameter. To account for the finite time for hadronization, we assume that the volume fraction of the quark-gluon plasma in the mixed phase varies linearly in time, i.e.,

$$f_q(t)=f_q^0\left[1-\frac{t}{\tau}\right]\ , \quad (19)$$

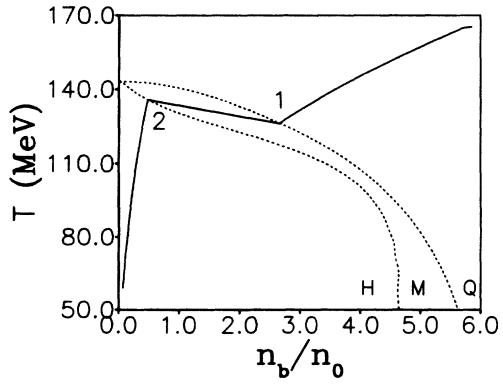

FIG. 5. The trajectory along which the system evolves in the nuclear phase diagram of Fig. 1 for collisions between two Ca nuclei at 14 GeV/nucleon.

where τ is the lifetime of the mixed phase that is taken to be an adjustable parameter. We see that the fireball is reheated during the phase transition because of the large latent heat as a result of the decrease of its density and the large difference in the entropy per baryon between the quark-gluon plasma and the hadronic matter.[21]

IV. CHEMICAL PROCESSES

In the quark-gluon phase, we neglect all the chemical processes and assume that the light quarks, antiquarks, and gluons are in both thermal and chemical equilibriums during the expansion of the quark-gluon matter. This should be a reasonable approximation as the process $q\bar{q}\leftrightarrow gg$ is fast. As in the consideration of the phase diagram, we shall also neglect strange quark production in the fireball. This will not change our results appreciably as it has been shown in Ref. 11 that the concentration of strange quarks remains small during the quark-gluon phase.

A. Chemical processes in hadronic phase

In the hadronic phase, we include the following processes:

$$NN\leftrightarrow N\Delta\ , \quad (20a)$$

$$\Delta\leftrightarrow N\pi\ , \quad (20b)$$

$$\pi\pi\leftrightarrow\rho\ . \quad (20c)$$

In the temperature regime, other hadronic resonances do not play important roles. Again, we have neglected the strange hadrons due to their relatively low concentrations. The source functions for these reactions are

$$\psi_N=-\langle\sigma_{\pi N}^{\Delta}v_{\pi N}\rangle n_\pi n_N+\Gamma_\Delta n_\Delta -\tfrac{1}{2}\langle\sigma_{NN}^{N\Delta}v_{NN}\rangle n_N^2+\langle\sigma_{N\Delta}^{NN}v_{N\Delta}\rangle n_N n_\Delta\ , \quad (21a)$$

$$\psi_\pi=-\langle\sigma_{\pi N}^{\Delta}v_{\pi N}\rangle n_\pi n_N+\Gamma_\Delta n_\Delta -\tfrac{1}{2}\langle\sigma_{\pi\pi}^{\rho}v_{\pi\pi}\rangle n_\pi^2+2\Gamma_\rho n_\rho\ , \quad (21b)$$

$$\psi_\Delta=\langle\sigma_{\pi N}^{\Delta}v_{\pi N}\rangle n_\pi n_N-\Gamma_\Delta n_\Delta +\tfrac{1}{2}\langle\sigma_{NN}^{N\Delta}v_{NN}\rangle n_N^2-\langle\sigma_{N\Delta}^{NN}v_{N\Delta}\rangle n_N n_\Delta\ , \quad (21c)$$

$$\psi_\rho=\tfrac{1}{2}\langle\sigma_{\pi\pi}^{\rho}v_{\pi\pi}\rangle n_\pi^2-\Gamma_\rho n_\rho\ , \quad (21d)$$

where Γ_Δ and Γ_ρ are the widths of the Δ and the ρ resonances, respectively. The average of the product of the cross section σ_{12}^{34} and the relative velocity v_{12} is defined as

$$\langle\sigma_{12}^{34}v_{12}\rangle=\int d^3\mathbf{k}_1\int d^3\mathbf{k}_2 f_1(\mathbf{k}_1)f_2(\mathbf{k}_2)\sigma_{12}^{34}v_{12}\ , \quad (22)$$

where $f_i(\mathbf{k}_i)$ is the normalized momentum distribution of the ith particle. For the cross sections $\sigma_{\pi N}^{\Delta}$ and $\sigma_{NN}^{N\Delta}$, we use those of Cugnon *et al.*,[27]

$$\sigma_{\pi N}^{\Delta}=\frac{12.62}{1+4[(s^{1/2}-1.232)/\Gamma_\Delta]^2}\ \text{fm}^2\ , \quad (23a)$$

$$\sigma_{NN}^{N\Delta}=\frac{2(s^{1/2}-2.015)^2}{0.015+(s^{1/2}-2.015)^2}\ \text{fm}^2\ , \quad (23b)$$

where the center-of-mass energy $s^{1/2}$ is in units of GeV. The cross section $\sigma^{\rho}_{\pi\pi}$ can be similarly parametrized by

$$\sigma^{\rho}_{\pi\pi}=\frac{27.9}{1+4[(s^{1/2}-0.770)/\Gamma_{\rho}]^2}\ \text{fm}^2\ . \tag{24}$$

The inverse cross sections are then determined from the detailed balance relations.

B. Combinatoric recombination model for hadronization

During the hadronization of the quark-gluon plasma through the mixed phase, gluons fragment into quark-antiquark pairs and quarks and antiquarks recombine into hadrons. For gluon fragmentation, we use the model of Koch *et al.*[8] Then the effective numbers of quarks and antiquarks are given by

$$\tilde{N}_q=N_q+f_l N_g,\quad \tilde{N}_{\bar{q}}=N_{\bar{q}}+f_l N_g\ , \tag{25}$$

with $f_l=f_u=f_d\simeq 0.425$ according to the string model.

The formation of quarks and antiquarks into hadrons can be determined by the combinatoric recombination model of Biró and Zimányi.[28] In this model, the number of baryons N_B, antibaryons $N_{\bar{B}}$, and mesons N_M are given by

$$N_M=\alpha\tilde{N}_q\tilde{N}_{\bar{q}},\quad N_B=\frac{1}{3!}\beta\tilde{N}_q^3,\quad N_{\bar{B}}=\frac{1}{3!}\beta\tilde{N}_{\bar{q}}^3\ . \tag{26}$$

The coefficients α and β are determined from the conservation of total baryon numbers and are

$$\alpha=\frac{4A}{3A^2+B^2},\quad \beta=\frac{8}{3A^2+B^2}\ , \tag{27}$$

with

$$A=\tilde{N}_q+\tilde{N}_{\bar{q}},\quad B=\tilde{N}_q-\tilde{N}_{\bar{q}}\ . \tag{28}$$

To determine the numbers of N, Δ, π, and ρ and their antiparticles we use the thermal equilibrium model and obtain the following ratios:

$$\frac{N_N}{N_{\Delta}}=\frac{N_N}{N_{\bar{\Delta}}}\approx\frac{d_N m_N^2 K_2(m_N/T)}{d_{\Delta}m_{\Delta}^2K_2(m_{\Delta}/T)}\ ,$$
$$\frac{N_{\pi}}{N_{\rho}}\approx\frac{d_{\pi}m_{\pi}^2K_2(m_{\pi}/T)}{d_{\rho}m_{\rho}^2K_2(m_{\rho}/T)}\ , \tag{29}$$

where d's and m's are the degeneracies and masses of the particles; K_2 is the modified Bessel function.

V. ELEMENTARY DILEPTON PRODUCTION PROCESSES

For dilepton production we take into account contributions from both $q\bar{q}$ and $\pi\pi$ annihilations and the neutron-proton bremsstrahlung, i.e.,

$$q\bar{q}\rightarrow e^+e^-\ , \tag{30a}$$
$$\pi\pi\rightarrow e^+e^-\ , \tag{30b}$$
$$np\rightarrow npe^+e^-\ . \tag{30c}$$

As the probability for dilepton production from these processes are small, they are treated perturbatively and do not affect the fireball expansion dynamics.

For a given invariant mass M of the dilepton, the production rate from $q\bar{q}$ annihilation is given by[14]

$$\frac{dR^{e^+e^-}_{q\bar{q}}}{dM}=\frac{40\alpha^2}{9(2\pi)^3}M^2TK_1(M/T)\left[1-\frac{4m_e^2}{M^2}\right]^{1/2}\left[1-\frac{4m_q^2}{M^2}\right]^{1/2}\left[1+\frac{2m_e^2}{M^2}\right]\left[1+\frac{2m_q^2}{M^2}\right]\ , \tag{31}$$

where α is the fine structure constant and $K_1(x)$ is the modified Bessel function.

Dilepton production from $\pi\pi$ annihilation is calculated according to[16]

$$\frac{dR^{e^+e^-}_{\pi\pi}}{dM}=\frac{8\pi\alpha^2n_{\pi}^2K_1(M/T)|F_{\pi}|^2}{3m_{\pi}^4M^2T[K_2(m_{\pi}/T)]^2}\times\sum_{k_i(\omega=M/2)}\frac{k_i^4}{\left|\frac{d\omega}{dk_i}\right|}|S_i|^2\ , \tag{32}$$

where F_{π} is the pion electromagnetic form factor that we take from Ref. 15, i.e.,

$$F_{\pi}(M)=\frac{m_{\rho}^4}{(m_{\rho}^2-M^2)^2+m_{\rho}^2\Gamma_{\rho}^2}+\frac{1}{4}\frac{m_{\rho'}^4}{(m_{\rho'}^2-M^2)^2+m_{\rho'}^2\Gamma_{\rho'}^2}\ , \tag{33}$$

with $m_{\rho}=775$ MeV, $\Gamma_{\rho}=155$ MeV, $m_{\rho'}=1600$ MeV, and $\Gamma_{\rho'}=260$ MeV. In Eq. (32), the pion dispersion relation $\omega(k)$ is given by,

$$\omega^2=\mathbf{k}^2+m_{\pi}^2+\mathbf{k}^2\Pi(\omega,\mathbf{k})\ , \tag{34}$$

where $\Pi(\omega,\mathbf{k})$ is the pion self-energy in the nuclear matter and can be calculated in the delta-hole model as in Ref. 16. The S_i is the pionic weighting factor and is determined by

$$S_i=\left[1-k_i^2\frac{\partial\Pi(\omega,k_i)}{\partial\omega^2}\right]^{-1}\ . \tag{35}$$

The rate for the process $np\rightarrow npe^+e^-$ is given by

$$\frac{dR^{e^+e^-}_{np}}{dM}=\frac{1}{4}\left\langle\frac{d\sigma^{e^+e^-}_{np}}{dM}v_{np}\right\rangle n_N^2\ , \tag{36}$$

with the dilepton production cross section evaluated in the soft-photon approximation corrected by the phase

space,[15] i.e.,

$$\frac{d\sigma_{np}^{e^+e^-}}{dM}=\frac{2\alpha^2}{3\pi^2}\frac{\bar{\sigma}(s)}{M}\ln\left[\frac{\sqrt{s}-2m_N}{M}\right]\frac{R_2(\sqrt{s_2})}{R_2(\sqrt{s})}. \quad (37)$$

In the above, $\bar{\sigma}(s)$ is the momentum transfer weighted nucleon-nucleon elastic cross section at a center-of-mass energy $\sqrt{s}$ and can be parametrized by

$$\bar{\sigma}(s)=\left[\frac{1.8\ (\mathrm{fm^2\,GeV})}{s-4m_N^2}+1.0\ \mathrm{fm}^2\right]\left[\frac{s}{4m_N^2}-1\right]. \quad (38)$$

The functions $R_2(\sqrt{s_2})$ and $R_2(\sqrt{s})$ are, respectively, the Lorentz invariant two-body phase-space integrals of the final two nucleons with and without the dilepton pair. For the former case, we have $s_2=s+M-2\sqrt{s}E$, with E being the energy of the dilepton in the center-of-mass frame. The factor $\frac{1}{4}$ in Eq. (36) accounts for the fact that we consider an isosymmetric system so that the neutron density is the same as the proton density and both are half of the nucleon density.

VI. RESULTS

A. Dilepton production from ^{40}Ca+^{40}Ca at 14 GeV/nucleon

As an illustration for understanding dilepton production in high-energy heavy-ion collisions, we have carried out a study of the central collision between two Ca nuclei at an incident energy of 14 GeV/nucleon. The trajectory in the phase diagram along which the system evolves has already been shown in Fig. 5. The time evolution of the system is determined by the hydrodynamical equation with the linear scaling *Ansatz*, corresponding to $n=1$ in Eq. (16), for the velocity profile. The lifetime τ of the mixed phase is taken to be 5 fm/c, which is similar to that of Ref. 29. We show in Fig. 6 the dilepton invariant mass spectrum. The long-dashed curve is the contribution from the $q\bar{q}$ annihilation in the quark-gluon plasma, while the dotted curve is from $\pi\pi$ annihilation in the hadronic matter. The two peaks in the latter correspond to the ρ resonances at 775 and 1660 MeV, respectively. It is seen that the former becomes important for dileptons with invariant masses larger than 2 GeV. At smaller invariant masses, it is still dominated by the $\pi\pi$ annihilation even though the corresponding hadronic matter is at a relatively low density of about n_0 after the complete hadronization from the initial quark-gluon plasma. Also shown in the figure by the short-dashed curve is the contribution from pn bremsstrahlung that is negligible compared to those from either $q\bar{q}$ or $\pi\pi$ annihilations. If we assume that no quark-gluon plasma is formed in the initial stage and that the initial matter is a dense hadronic matter of density of also about $6n_0$, then the dilepton invariant mass spectrum from $\pi\pi$ annihilation is given by the solid curve in Fig. 6. We see that the dilepton yield is much larger than that from the scenario of the formation of an initial quark-gluon plasma. This is because of the higher hadronic matter density and temperature of the fireball in the latter case.

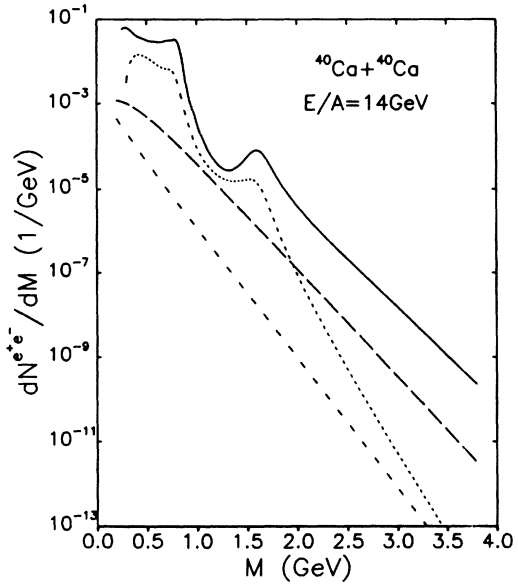

FIG. 6. Dilepton invariant mass spectra from the central collision of Ca on Ca at 14 GeV/nucleon. The long-dashed curve is from the $q\bar{q}$ annihilation in the quark-gluon plasma while the dotted and short-dashed curves are, respectively, from the $\pi\pi$ annihilation and the pn bremsstrahlung in the hadronic phase. The solid curve is from the $\pi\pi$ annihilation in the scenario that no quark-gluon plasma is formed in the collision.

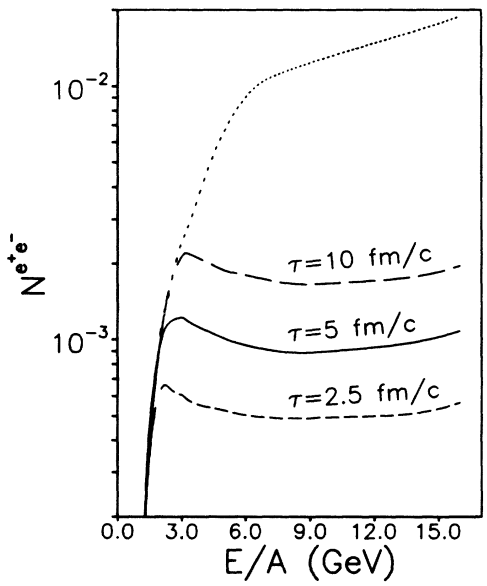

FIG. 7. The total dilepton yield for invariant masses between $2m_\pi$ and 1 GeV as a function of the incident energy per nucleon for the central collision of Ca on Ca. The solid curve is from initial fireball conditions determined from the phase diagram of Fig. 1 and a mixed-phase lifetime $\tau=5$ fm/c. The dotted curve is from assuming that the fireball is initially always in the hadronic phase. The short- and long-dashed curves correspond to $\tau=2.5$ and 10 fm/c, respectively.

B. Integrated dilepton excitation function from heavy-ion collisions

Since the total dilepton yield with invariant masses $2m_\pi < M < 1$ GeV is dominated by $\pi\pi$ annihilation, it would increase significantly with the initial density of the hadronic matter due to both the increasing softening of the pion dispersion relation and the increasing initial temperature with increasing density. In Fig. 7, we show such an excitation function for this yield. It is calculated with the hydrochemical model as before for the reaction of ^{40}Ca on ^{40}Ca at zero impact parameter corresponding to central collisions. The solid curve is obtained when the initial conditions of the fireball is determined from the phase diagram of Fig. 1. It shows a steep rise of the dilepton yield at incident energies below about 2 GeV/nucleon as the initial hadronic matter density increases as a result of higher compression. When the initial energy density is large enough so that a mixed phase of quark-gluon and hadronic matter is formed, the dilepton yield is seen to decrease as a function of the incident energy. Also shown in the figure by the dotted curve is the dilepton yield from assuming that the initial fireball is always in the hadronic phase. As in Fig. 6, the dilepton yield at a given incident energy is higher in the latter case than that from the case when either a mixed or a quark-gluon phase exists. Because of the short formation time of the initial fireball, it is likely that the system may be superheated and still stays in the hadronic phase even though its energy density is high enough to be in the mixed phase. We thus expect that the steep rise of the dilepton excitation function would continue to higher incident energies. In either case, the onset of the formation of a quark-gluon plasma in the initial high-density matter is accompanied by a saturation in the total yield of the dilepton with invariant masses $2m_\pi < M < 1$ GeV.

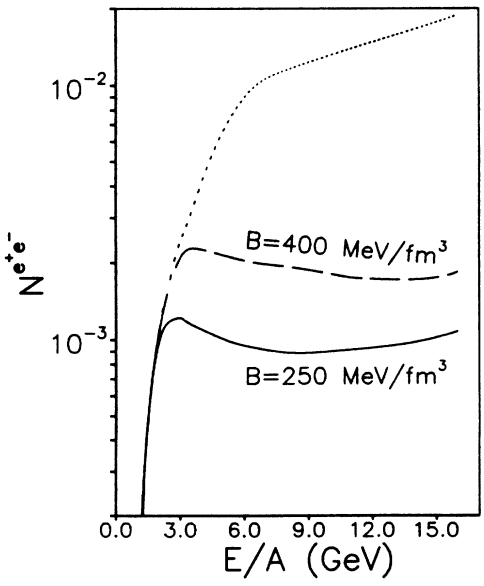

FIG. 8. Same as Fig. 7 with the long-dashed curve obtained from the phase diagram of Fig. 3 with a bag constant of 400 MeV/fm^3.

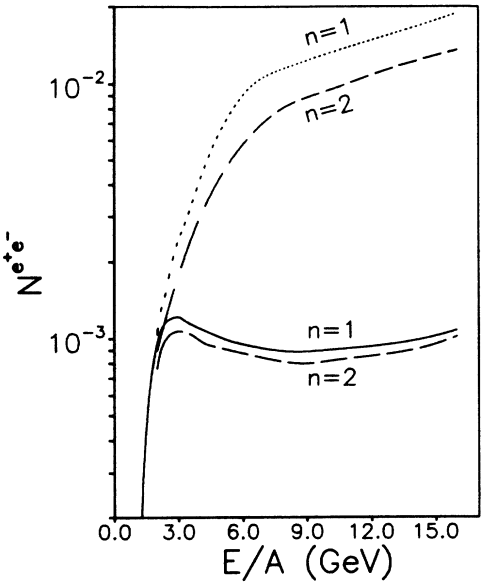

FIG. 9. Same as Fig. 7 for two different *Ansätze* for the velocity profile of the fireball.

These results are not qualitatively modified when different phase diagrams and hydrodynamical descriptions are used. The short-dashed and long-dashed curves, corresponding to lifetimes for the mixed phase $\tau = 2.5$ fm/c and $\tau = 10$ fm/c respectively, still show the saturation of dilepton when a baryon-rich quark-gluon plasma is formed. The same is true as shown by the long-dashed curve in Fig. 8 if we use a phase diagram obtained with a larger bag constant of 400 MeV/fm^3, which leads to a critical energy density of ≈ 2 GeV/fm^3 for the formation of the quark-gluon plasma. Using a quadratic scaling *Ansatz* for the velocity profile in the hydrodynamical expansion leads to only minor changes in the dilepton excitation function as shown in Fig. 9. We therefore conclude that the saturation of dilepton yield due to the formation of a baryon-rich quark-gluon plasma remains under these variations of the model.

VII. SUMMARY AND CONCLUSIONS

Motivated by the search for signatures for the formation of a quark-gluon plasma in high-energy heavy-ion reactions, we have studied dilepton production from such reactions. In particular, we have considered heavy-ion collisions in an energy regime available at the Brookhaven AGS. We have assumed that an initial high-density fireball is formed and its expansion is described by a simplified relativistic hydrodynamical model. Dileptons are then mainly produced from $q\bar{q}$ and $\pi\pi$ annihilations. Because of the strong p-wave pion-nucleon interaction, the pion spectrum in the nuclear matter is modified and has been taken into account via the delta-hole model. We have found that the dilepton yield at invariant masses between $2m_\pi$ and 1 GeV is reduced substantially if a baryon-rich quark-gluon plasma is formed

in the initial stage of the collisions. This effect is largely due to the higher initial hadronic density in the hadronic scenario than that after the hadronization in the quark-gluon scenario. Since this is a general feature of the nuclear phase diagram, we expect that the present result will still hold if other nuclear phase diagrams are used in the calculation. In the present study, we have ignored the decay of the rho meson into dilepton since its contribution has already been included through the pion-pion annihilation. We have also neglected the contribution to dilepton production from delta decay and pion-nucleon interaction as they are not important in high-energy nuclear reactions.[30] Experiments carried out so far at the Bevalac[31,32] are very useful in verifying the effect of the softening of the pion spectrum in dense nuclear matter on dilepton production through $\pi\pi$ annihilations. Future experiments at the AGS on dilepton production will be extremely interesting in searching for evidence for the formation of a baryon-rich quark-gluon plasma in the initial stage of the collision. Further theoretical studies are certainly required not only in repeating the present calculation with more sophisticated models for the nuclear phase diagram but also in investigating the effect of dilepton production before thermalization on the signature proposed here. The latter is especially needed in view of the recent result from the relativistic quantum molecular dynamics[33] in which it is claimed that preequilibrium effects are very important for kaon production in heavy-ion collisions at the AGS energies.

ACKNOWLEDGMENTS

This work was supported in part by the National Science Foundation under Grant Nos. PHY-8608149 and PHY-8907986, and the Robert A. Welch Foundation under Grant No. A-1110.

*Permanent address: Physics Department, Nankai University, Tianjin, People's Republic of China.

[1] *Quark Matter '88, Proceedings of the Seventh International Conference on Ultrarelativistic Nucleus-Nucleus Collisions,* edited by G. Baym, P. Braun-Munzinger, and S. Nagamiya [Nucl. Phys. **A498**, 1c (1989)].

[2] Proceedings of the Second Workshop on Experiments and Detectors for a Relativistic Heavy Ion Collider (RHIC), Lawrence Berkeley Laboratory, 1987 (Lawrence Berkeley Laboratory Report No. LBL-24604, 1987).

[3] M. C. Chu and T. Matsui, Phys. Rev. D **37**, 1851 (1988).

[4] S. Gavin, M. Gyulassy, and A. D. Jackson, Phys. Lett. **207**, 257 (1988).

[5] C. Gerschel and J. Hüfner, Phys. Lett. B **207**, 253 (1988).

[6] R. Vogt, M. Prakash, P. Koch, and T. H. Hansson, Phys. Lett. **207**, 263 (1988).

[7] J. Stachel and P. Braun-Munzinger, Phys. Lett. B **216**, 1 (1989).

[8] P. Koch, B. Müller, and J. Rafelski, Phys. Rep. **142**, 167 (1986).

[9] Y. Miake, Bull. Am. Phys. Soc. **32**, 1565 (1987); T. Abbott *et al.*, Nucl. Phys. **A498**, 67c (1989).

[10] C. M. Ko and L. H. Xia, Phys. Rev. C **37**, 179 (1988); Nucl. Phys. **A498**, 561c (1989).

[11] L. H. Xia and C. M. Ko, Phys. Lett. B **222**, 343 (1989).

[12] S. A. Chin, Phys. Lett. **119B**, 51 (1982).

[13] P. J. Siemens and S. A. Chin, Phys. Rev. Lett. **55**, 12 (1985).

[14] K. Kajantie, J. Kapusta, L. McLerran, and A. Mekjian, Phys. Rev. D **34**, 811 (1986); **34**, 2746 (1986).

[15] C. Gale and J. Kapusta, Phys. Rev. C **35**, 2107 (1987).

[16] L. H. Xia, C. M. Ko, L. Xiong, and J. Q. Wu, Nucl. Phys. **A485**, 721 (1988).

[17] C. M. Ko, L. H. Xia, and P. J. Siemens, Phys. Lett. B **231**, 16 (1989).

[18] N. Glendenning, Lawrence Berkeley Laboratory Report No. LBL-25956, 1989.

[19] C. M. Ko and L. H. Xia, Phys. Rev. Lett. **62**, 1595 (1989).

[20] U. Heinz, K. S. Lee, M. J. Rhodes-Brown, Phys. Rev. Lett. **58**, 2292 (1987).

[21] K. S. Lee, M. J. Rhodes-Brown, and U. Heinz, Phys. Lett. B **174**, 123 (1986).

[22] B. Müller, in *The Physics of the Quark-Gluon Plasma,* Vol. 225 of *Lecture Notes in Physics,* edited by H. Araki, J. Ehlers, K. Hepp, R. Kippenhahn, H. A. Weidenmüller, and J. Zittartz (Springer-Verlag, Berlin, 1985).

[23] U. Heinz, P. R. Subramanian, H. Stöcker, and W. Greiner, J. Phys. G **12**, 1237 (1986).

[24] B. D. Serot and H. Uechi, Ann. Phys. (N.Y.) **179**, 272 (1987).

[25] N. K. Glendenning, Phys. Rev. C **37**, 2733 (1988).

[26] T. S. Biró, H. W. Barz, B. Lukács, and J. Zimányi, Phys. Rev. C **27**, 2695 (1983).

[27] J. Cugnon, D. Kinet, and J. Vandermeulen, Nucl. Phys. **379**, 553 (1982).

[28] T. S. Biró and J. Zimányi, Nucl. Phys. **A395**, 525 (1983).

[29] H. W. Barz, B. L. Friman, J. Knoll, and H. Schulz, Nucl. Phys. **A484**, 661 (1988).

[30] L. Xiong, J. Q. Wu, Z. G. Wu, and C. M. Ko (submitted to Phys. Rev. C).

[31] G. Roche *et al.*, Phys. Rev. Lett. **61**, 1069 (1988).

[32] C. Naudet *et al.*, Phys. Rev. Lett. **62**, 2652 (1989).

[33] R. Mattiello, H. Sorge, H. Stöcker, and W. Greiner, Phys. Rev. Lett. **63**, 1459 (1989).